Electronic Supplementary Material (ESI) for Nanoscale Advances.

Supporting Information

A novel zinc sulfide impregnated carbon composite derived from Zeolitic Imidazolate Framework-8 for sodium-ion hybrid solid-state flexible capacitor

Vishal Shrivastav[1,2,$], Shashank Sundriyal[1,$,#], Priyanshu Goel[1,2], Avishek Saha[1], Umesh K. Tiwari[1,2*], Akash Deep[1,2*]

[1]CSIR-Central Scientific Instruments Organisation (CSIR-CSIO), Chandigarh-160030, India; [2]Academy of Scientific and Innovative Research (AcSIR-CSIO), Ghaziabad-201002, India

[#]Present Address: CSIR-National Physical Laboratory (CSIR-NPL), New Delhi, India:

*Correspondence: dr.akashdeep@csio.res.in, umeshtiwari@csio.res.in

[$]Both authors contributed equally

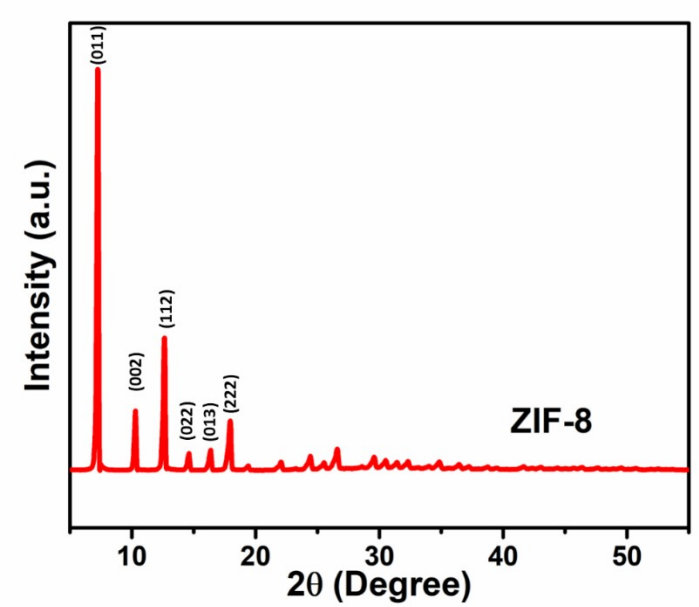

Figure S1. XRD pattern of ZIF-8.

Figure S1 shows the XRD pattern of ZIF-8 (used as a sacrificial template). The high intensity diffraction peaks demonstrate a crystalline nature of ZIF-8. The observed peaks are associated to the planes 011, 002, 112, 022, 013, and 222 plane. The data are in good agreement with the previously reported XRD patterns of ZIF-8.[1]

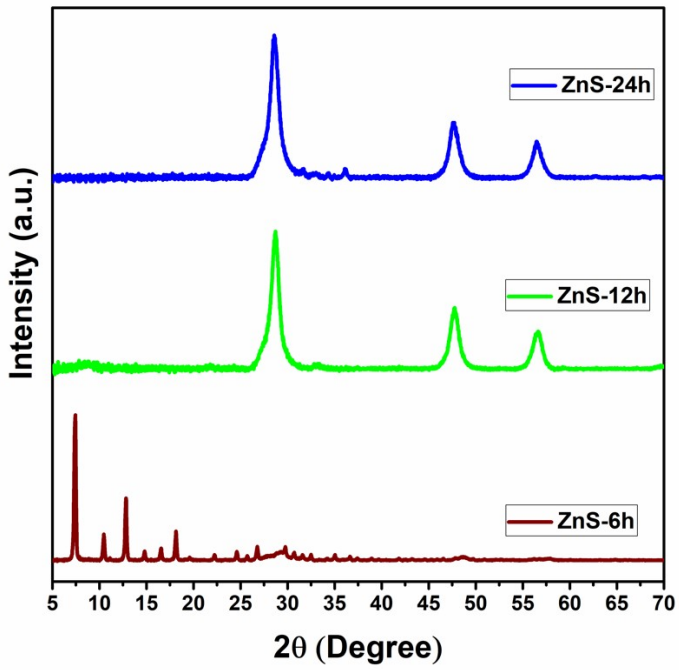

Figure S2. XRD pattern of bare ZnS product synthesized for a different time periods.

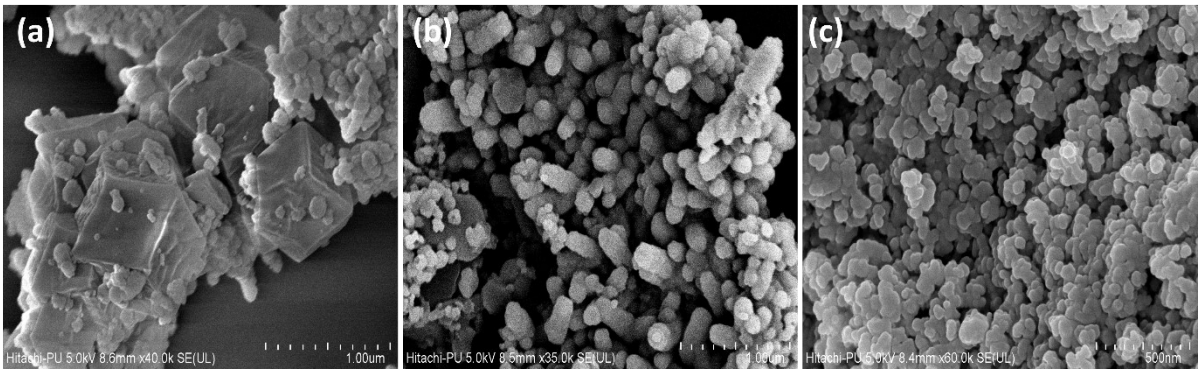

Figure S3. FESEM images of bare ZnS product, synthesized via the hydrothermal treatement for different time periods, e.g., (a): 6 h, (b) 12 h, (c) 24 h.

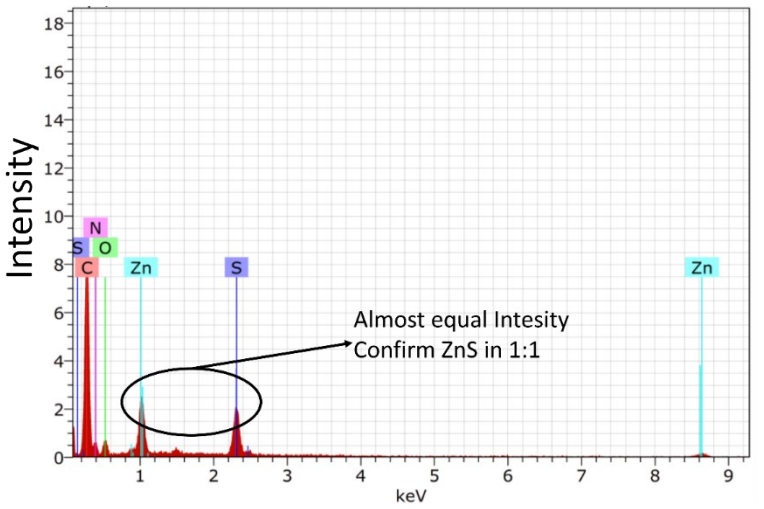

Element	Series	unn. C [wt.%]	norm. C [wt.%]	Atom. C [at.%]	Error (3 Sigma) [wt.%]
Carbon	K-series	77.39	59.97	70.11	31.84
Oxygen	K-series	11.37	8.81	7.73	7.80
Sulfur	K-series	5.55	4.30	1.88	0.75
Zinc	K-series	10.99	8.52	1.83	2.14
Nitrogen	K-series	23.75	18.40	18.45	16.55
Total:		129.06	100.00	100.00	

1:1

Figure S4. EDS analysis of ZnS loaded carbon (ZLC)

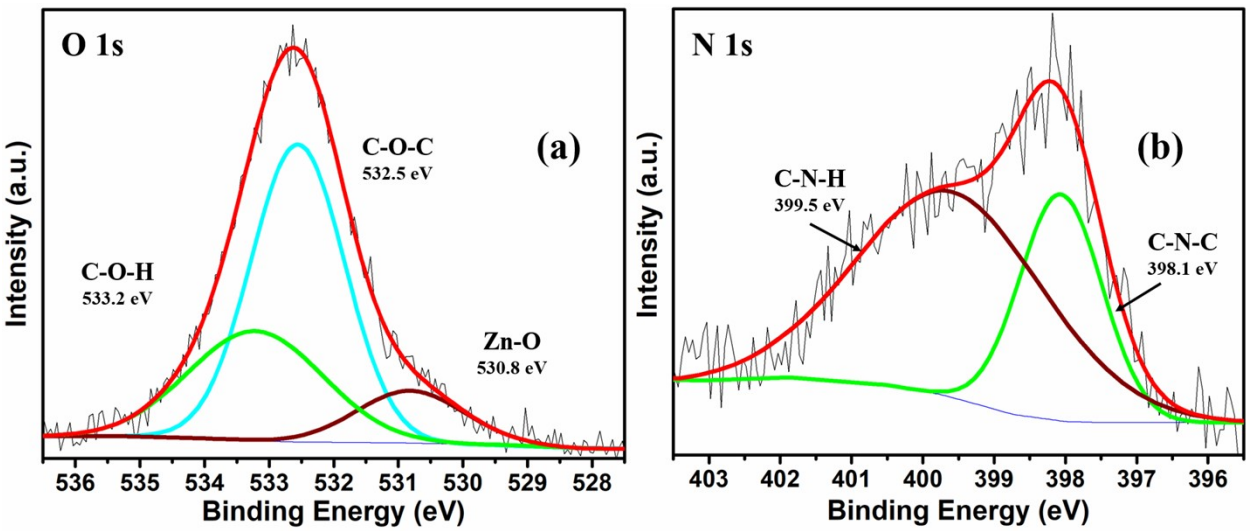

Figure S5. High-resolution XPS spectra of ZLC-800. (a): O1s; (b): N1s.

S1.1. Experimental

S1.2.1. Materials

All the materials used in this manuscript were of analytical grade and used without any further purification. Zinc acetate, PVDF, carbon black, thiourea, and 2-methylimidazole were purchased from Merck, India. The solvents like methanol and N-methyl pyrrolidone (NMP) were purchased from Himedia, India.

S1.2.2. Synthesis

S1.2.2.1. Synthesis of ZIF-8

ZIF-8 was prepared using a method reported elsewhere.[2] Briefly, 585 mg of zinc acetate was dissolved in 4 mL of deionized (DI) water. In another vessel, 11.22 g of 2-methyimidazole was suspended in 40 mL of DI water. These above two solutions were mixed and the resulting solution instantly turned into a white colored suspension, indicating the nucleation of the ZIF-8 crystals. The mixture was kept on stirring at room temperature conditions for 6 h. Thereafter, a centrifugtion step (8000 RPM) was performed to collect the formed ZIF-8 crystals. The product was washed with DI water and methanol to remove the unreactive residues. It was left to dry overnight in a vacuum oven at 80 °C.

S1.2.2.2. Synthesis of Zn ion infused carbon (ZIC-n, n = pyrolyzing temperature)

The ZIF-8 MOF has been pyrolyzed at three different temperatures under the inert Ar atmosphere to obtain zinc infused carbon (ZIC-n). For this, a known amount of ZIF-8 was taken in an alumina boat which was then placed in the center of a tube furnace. The sample was treated at three different temperatures, i.e., 700, 800, and 900 °C). The temperature was increased with a

ramp rate of 5 °C/min. Once the temperature reached to the desired level, the furnace was allowed to operate for 4 h. After the experiment, the furnace cooled down to room temperature at the same (5 °C/min) ramp rate. Upon above heat treatment steps, ZIF-8 crystals collapsed to leave behind a mix phase of zinc infused carbon (ZIC-n).

S1.2.2.3. Conversion of ZIC-n into zinc free carbon (ZFC) for application as a negative electrode in supercapacitor

The known amounts of ZIC-n were mixed with a 2 M HCl solution and then stirred. This step leached out the content of zinc metal from the ZIC-n samples. The above treatement resulted in the recovery of zinc free carbon product (ZFC-n), which was subsequently washed with DI water till we obtained a filtrate of neutral pH. The ZFC-n samples were characterized for their surface area values and it was found that the ZFC-800, recovered by acid leaching treatement of ZIC-800, possessed a larger value of surface area than ZFC-700 and ZFC-900.

S1.2.2.4. Conversion of ZIC-n into zinc loaded carbon (ZIC) for application as a positive electrode in supercapacitor

As mentioned in the preceeding subsection, the ZIC-800 intermediate yielded the preparation of ZFC-800, which had the highest surface area value. This observation was an indicator that among the three intermediate compounds, i.e., ZIC-800, ZIC-800, and ZIC-800, the ZIC-800 would possess the largest surface area and better porous characteristics. Therefore, this sample (ZIC-800) was also selected for the preparation of the ZnS loaded carbon (ZLC) composite. A known amount (100 mg) of ZIC-800 was dispersed in 10 mL of ethanol and then subject to ultrasonication for 30 min. In another beaker, 500 mg of thiourea was dissolved in 40 mL of DI water. Both the above solutions were mixed thoroughly and then transferred in a Teflon-lined

stainless steel autoclave for further thermal treatment at 120 °C for 24 h. After cooling down to the room temperature, the product (ZLC) was separated out by a filtration step and then washed several times with DI water and ethanol to remove the unreacted thiourea residue. The obtained ZLC product was dried overnight in a vacuum oven at 60 °C.

S1.2.2.5. Synthesis of bare xinc sulfide for comparative studies

For the purpose of some comparative studies, bare ZnS has also been synthesized. For this, 100 mg of ZIF-8 and 500 mg of thiourea, mixed in DI water, were allowed to react in a Teflon-lined stainless steel autoclave at 120 °C for 6, 12, or 24 h. Based on the characterization results obtained with FESEM and XRD, it was found that the above reaction of 6 or 12 did not lead to the complete transformation of ZIF-8 into ZnS nanoparticles. A reaction time of 24 h was found suitable to achieve the synthesis of pure ZnS nanoparticles which were free from any trace of the ZIF-8 phase. The obtained ZnS nanoparticles was washed several times with DI water and ethanol to remove unreacted thiourea and finally left to dry in a vacuum oven at 60 °C. The dried ZnS nanoparticles were further homogenized into a fine powder by careful milling in a mortar-pestle.

S1.2.3. Electrochemical studies

The electrochemical studies in a three-electrode setup were carried out using 1 M Na_2SO_4 as the electrolyte solution. For the preparation of working electrodes, the active material (e.g., ZLC, ZFC, or ZnS NPs) was converted into a slurry using NMP as a solvent. During the process, fractions of PVDF binder and carbon black were also added. The fraction ratio (wt %) of the active material and additives was maintained as follows: 80% active material, 10%, PVDF, 10% carbon black. The formed slurries were coated over a graphite foil (1.5 x 1.5 cm^2 coverage area)

by the drop-casting method. The prepared electrodes were dried for mainaining a proper adhesion of the material.

The electrochemical studies in the three-electrode setip were carried out using platinum wire (counter), Ag/AgCl (reference), and modified graphite foil current collector (working) electrodes. The cyclic voltammetry (CV) and galvanostatic charge-discharge (GCD) techniques were employed to determine the different electrochemical parameters, e.g., potential window, specific capacitance, cyclic stability, etc. The electrochemical impedance spectroscopic studies (EIS) were also performed in a three-electrode setup within the frequency range of 1 MHz to 0.1 Hz keeping an AC amplitude of 10 mV.

S1.2.4. Fabrication of hybrid asymmetrical supercapacitor device (HASD)

The positive (ZLC) and negative (ZFC) electrode materials were coated over the graphite foil (effective coverage area of 2 x 2 cm^2) after ensuring the required mass balance, as mentioned in the main text. The ZLC coated positive and ZFC coated negative electrodes were then sandwiched in the presence of PVA-1M Na_2SO_4 gel electrolyte to prepare an all-solid-state hybrid asymmetrical supercapacitor device (HASD). The CV, GCD, and EIS data were collected from the two-electrode HASD device to evaluate its electrochemical performance in terms of voltage window, specific capacitance, cyclic stability, energy density, and power density.

S1.2.5. Calculations of electrochemical parameters

The CV and GCD data have been used to calculate specific capacitance as per the following equations-

(i) CV based calculations [2]

$$C_s = \frac{1}{2msΔV}\int_{V_i}^{V_f} I(V)dV \quad \text{(S1)}$$

where ($\int IdV$) is the integral area of the CV curve, m is the mass of the active material, ΔV is the potential window of the material and s is the scan rate.

(ii) GCD based calculation

$$C_s = \frac{\Delta t \times I_d}{m \times \Delta V} \quad \text{(S2)}$$

Where, Δt is the discharging time, I_d is the discharge current density, m is the mass of active materials on the electrode in g, and ΔV is the voltage window.

(iii) Estimation of energy and power densities for HASD device (two-electrode system)

The energy density (E_d) and power density (P_d) are calculated using the following formulae[3],

$$E_d = \frac{C_s \times \Delta V_D^2}{2 \times 3.6} \quad \text{(S3)}$$

$$P_d = \frac{E_s \times 3600}{\Delta t} \quad \text{(S4)}$$

where, C_s = specific capacitance, Δt = discharging time, ΔV = total potential deviation of the voltage window

(iv) Relaxation time calculation

The relaxation time of the supercapacitor can be calculated from the variation of real and imaginary power in the system as a function of the variation in frequency. The power of the system can be expressed in terms of imaginary and real power terms as follows:

$S(\omega) = P(\omega) + jS(\omega)$ (S5)

where *P(ω)* and *S(ω)* are the function of imaginary and real capacitance, respectively. By bringing the change in applied voltage ($\Delta \mathbf{V_{rms}}$) in consideration, the *P(ω)* and *S(ω)* can be further expressed as follows:

$$P(\omega) = \omega C''(\omega)|\Delta \mathbf{V_{rms}}|^2 \quad \text{(S6)}$$

$$S(\omega) = \omega C'(\omega)|\Delta \mathbf{V_{rms}}|^2 \quad \text{(S7)}$$

where *C′* and *C″* are the real and imaginary parts of capacitance depending on the real and imaginary part of impedance, and $\boldsymbol{V_{rms}}$ is the ac perturbation applied potential. The equations to calculate C′ and C″ are given as follows:

$$C' = -Z''(\omega)/\omega|Z|^2 \quad \text{(S8)}$$

$$C'' = -Z'(\omega)/\omega|Z|^2 \quad \text{(S9)}$$

where *Z'* and *Z''* are the real and imaginary part of the impedance and *Z* is the combination of the real and imaginary parts of impedance, given by the following equation.

$$Z(\omega)^2 = (Z'(\omega))^2 + (Z''(\omega))^2 \quad \text{(S10)}$$

S2.1. Important charcterizations of ZFC (negative electrode material)

S2.1. Characterizations

The ZIF-8 derived zinc free carbon (ZFC) has been used as a negative electrode material for HASD. The different ZFC-n materials (n = pyrolysis temperature used to prepare ZIC-n intermediate) have been characterized with BET surface area test to determine the surface area and average pore size. From the BET surface area analyses of the different ZFC samples, the ZFC-800 sample yielded the maximum specific surface area of 535 m^2/g compared to the other two samples (ZFC-700 (408 m^2/g) and ZFC-900 (158 m^2/g)). Therefore, the ZFC-800 sample was concluded to be a more suitable option which could support the best electrolyte absorption within the pores of the material. Based on the above results, ZFC-800 sample was chosen as a

negative electrode material for the assembly of the HASD. From the FESEM analysis of ZFC-800, it can be concluded that polyhedron type morphology of the ZFC-800 sample (**Figure S6b**) resembled to that of ZIF-8. Most of the particles were formed in a size range of 200 nm to 1 μm.

Table 1: Surface area and pore size characterstics of ZFC-n samples through N_2 adsorption-desorption characterization

Sample	Surface area (m^2/g)	Mean pore diameter (nm)
ZFC-700	408	1.7
ZFC-800	535	7
ZFC-900	158	1.5

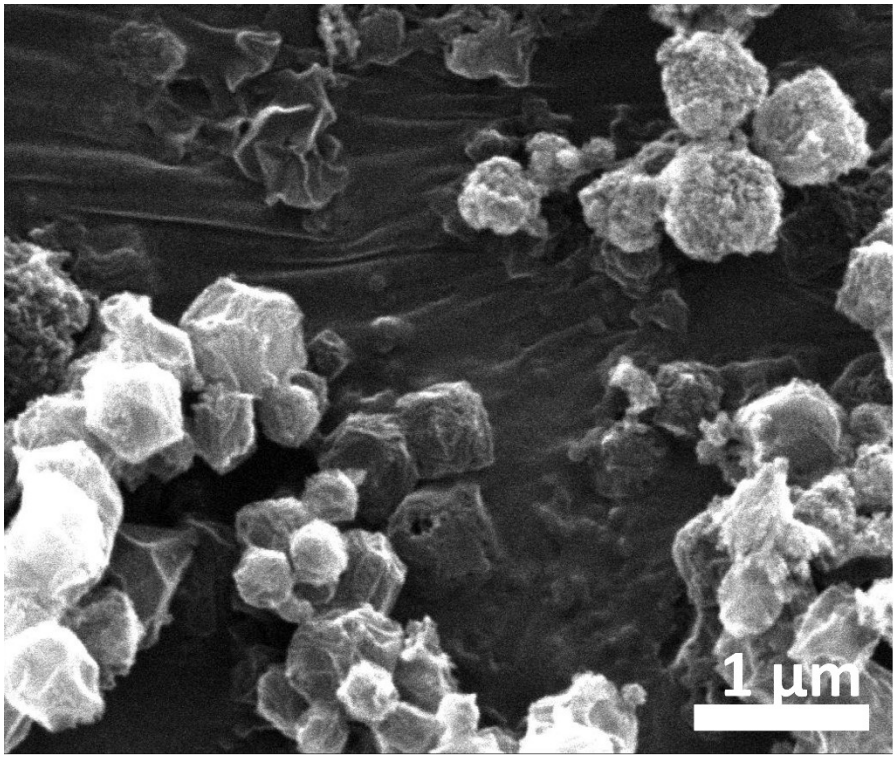

Figure S6. SEM image of ZFC-800 sample.

S2.2. Electrochemical performance

The potential window of the ZFC-800 electrode was identified by performing the CV of the electrodes in the presence of 1 M Na_2SO_4 electrolyte. This experiment was conducted up to a total potential window of 0.9 V (0.1 V to -0.8 V) because 1 M Na_2SO_4 can support a maximum voltage window of 1.23 V. The application of a broader voltage window with 1 M Na_2SO_4 can cause the decomposition of electrolyte resulting in a loss of electrolyte concentration and poor cycle stability. **Figure S7a** shows the CV curves of the ZFC-800 electrode at different scan rates. Most of the curves were rectangular to highlight the EDLC based charge storage in ZFC-800. A horizontal current profile indicated a low polarization resistance.[6] The voltammograms of ZFC-700 and ZFC-900 electrodes exhibited lesser area under curve than the ZFC-800 electrode. Therefore, it can be concluded that ZFC-800, possessing the largest surface area, could deliver maximum value of capacitance (**Figure S7b**).

ZFC-800 contained both amorphous and graphitic type carbon to allow effective electronic transport, which has resulted in an excellent electrochemical performance compared to ZFC-700 and ZFC-900. The fast-electronic transport and low charge transfer resistance in the ZFC-800 electrode was also confirmed by the recorded Nyquist plots of all the three samples (**Figure S7c**). The ZFC-800 electrode exhibited an effective series resistance (R_s) of 4.98 **Ω**. As there was no particular appearance of a semicircle, it indicated fast electron transfer and low charge transfer resistance. The EIS characteristcs of the ZFC-700 and ZFC-900 are also shown in **Figure S7c**. They showed higher ESR value than the ZIF-800, caused by a lower graphitic

carbon content. Upon comparing ZFC-700 and ZFC-900, the latter showed better conductivity as it had a small fraction of graphitic carbon. ZFC-700 contained carbon mostly in an amorphous form. The presence of graphitic phase carbon in the ZFC samples was directly related with the values of charge transfer resistances. Further, apart from graphitic carbon, ZFC-800 also contained the amorphous phase which proved beneficial from the electrochemical point of view. While the graphitic carbon provided a low resistance to support the fast electronic charge transfer, the amorphous carbon phase with its high specific surface area and well-distributed pores of meso and micro sizes facilitated better diffusion of electrolyte.

In view of the excellent electrochemical properties of ZFC-800, it was chosen as a negative electrode material for HASD. The GCD tests carried out to assess the specific capacitance at different current densities as shown in **Figure S7d**. A maximum specific capacitance of 200 F/g was attained at a current density of 1 A/g. In comparison, the ZFC-700 and ZFC-900 electrodes delivered lower discharging times (**Figure S7e**). The specific capacitance of the ZFC-800 electrode at different current densities is summarized in **Figure S7f**.

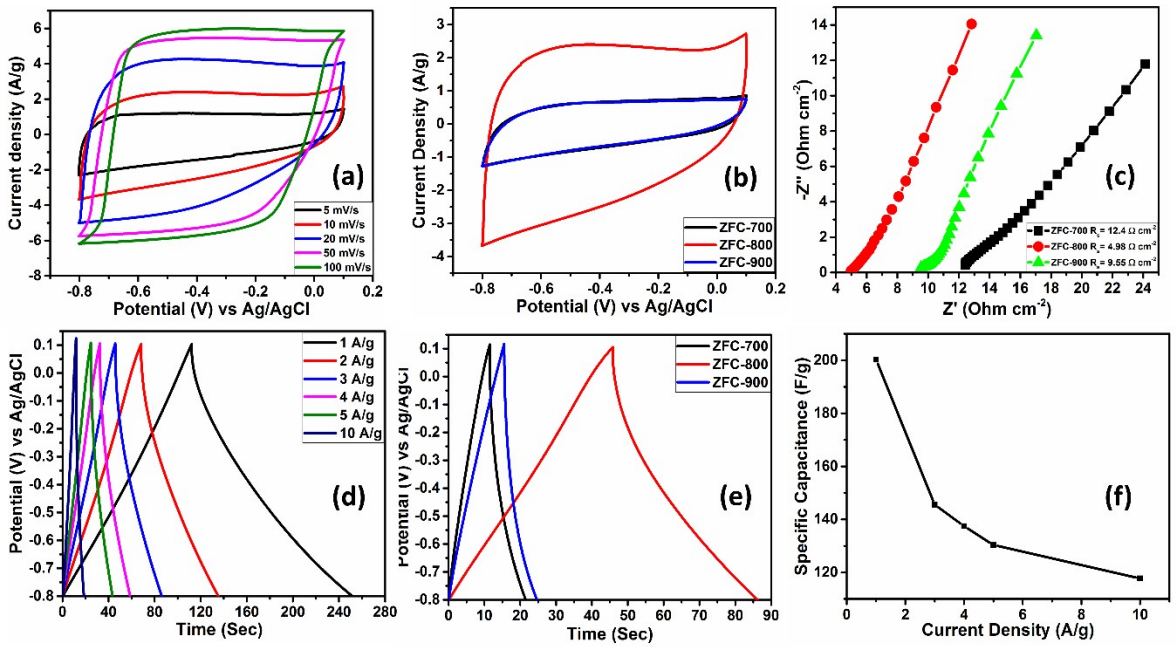

Figure S7. Electrochemical characterizations of ZFC-n samples. (a): CV curves of ZFC-800 at different scan rates; (b): Comparison of CV profiles of ZFC-700, ZFC-800, ZFC-900 at scan rate of 5 mV/s; (c): Nyquist plots ZFC-700, ZFC-800, ZFC-900 electrodes; (d): GCD curves of ZFC-800 electrode at various current densities; (e): Comparative GCD profiles of ZFC-700, ZFC-800, ZFC-900; (f): Variation of specific capacitance of ZFC-800 electrode as a function of current density.

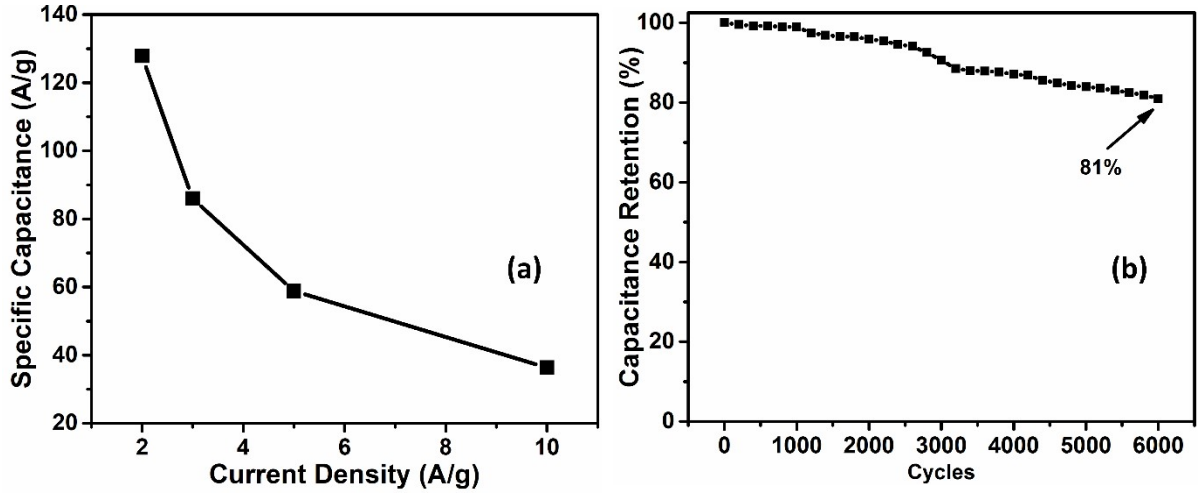

Figure S8. (a): Variation of specific capacitance of ZLC as a function of current density; (b): Cycle stability of ZLC during 6000 charging-discharging cycles.

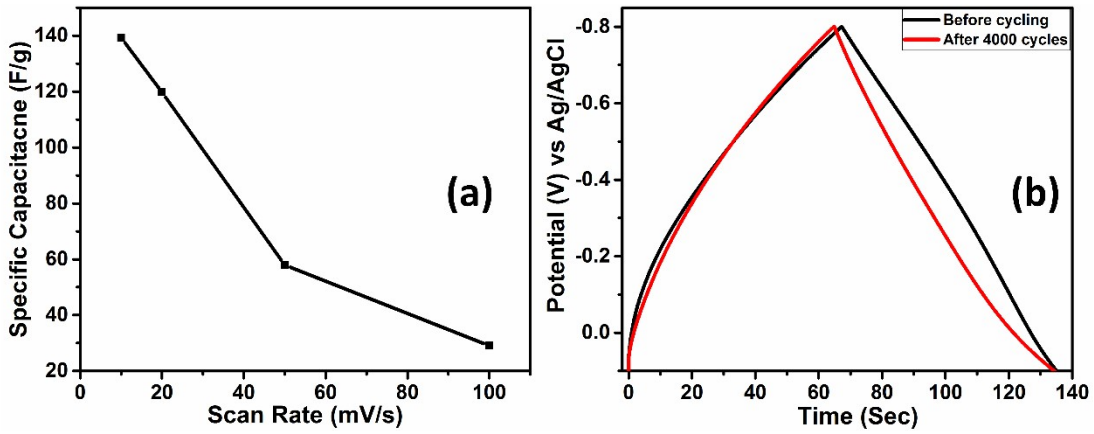

Figure S9. (a): Specific capacitance of ZFC-800 electrode upon varying the scan rate; (b): GCD curves of ZFC-800 electrode before and after 4000 nos. of charging-discharging cycles.

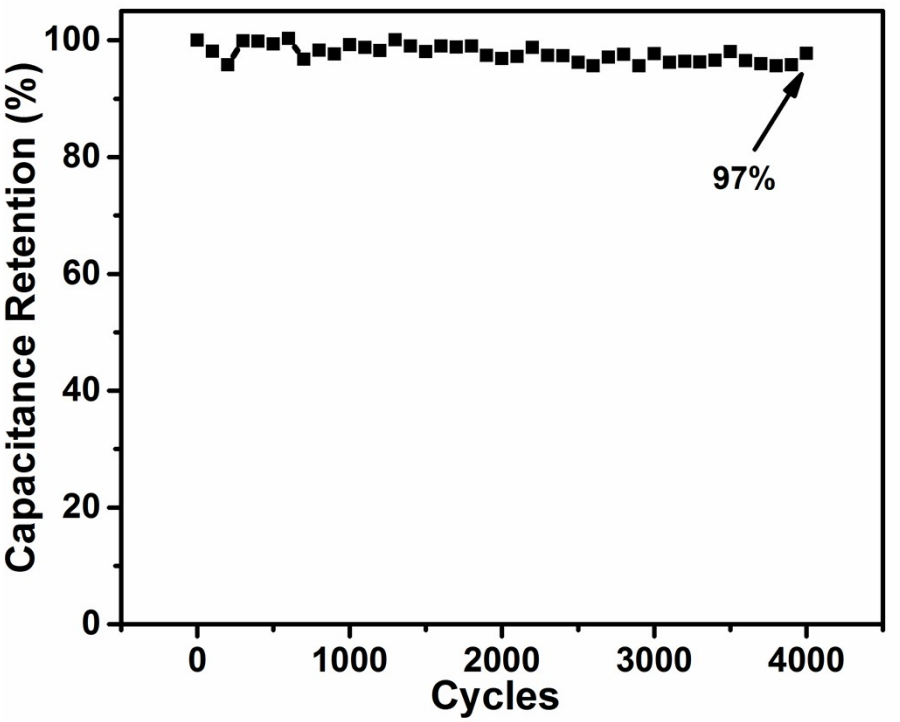

Figure S10. Cycle stability of ZFC-800 electrode during 4000 nos. of charging/discharging cycles.

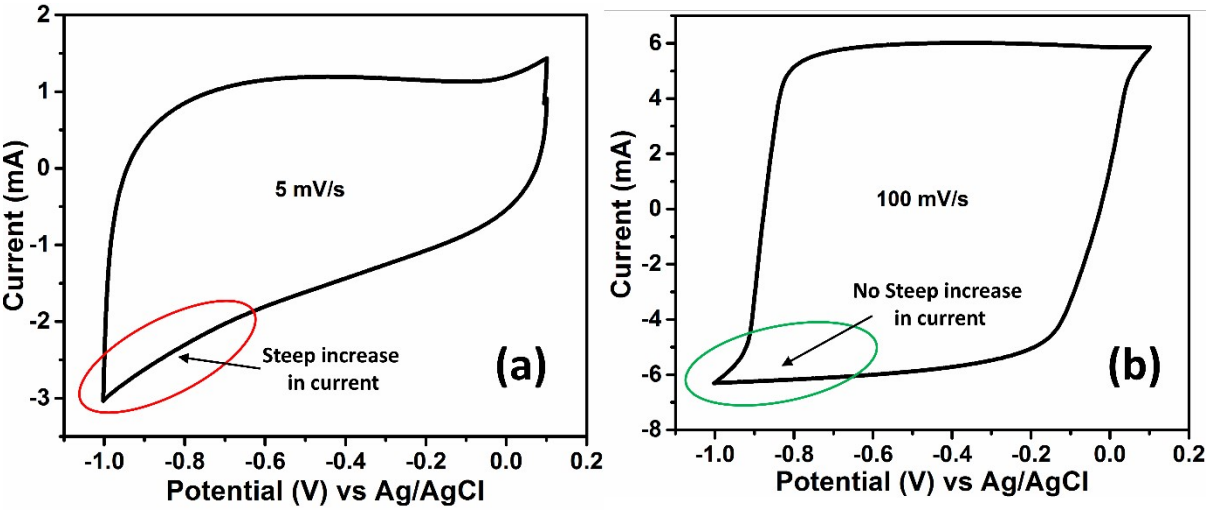

Figure S11. CV curves of ZFC-800 electrode at different scan rates. (a): 5 mV/s; (b): 100 mV/s.

To investigate any evolution of H_2 or O_2 gas during the opration of ZFC-800 electrode (negative electrode) at slow and fast scan rates, the studies were carried out in an extended negative

potential window (0.1 to -1 V). As seen in **Figure S12a**, a steep increase in current values was observed at low potential (< -0.8 V). This reflected the evolution of gas at the electrode surface. The above observantion can be explained by the fact that the operation at low potential allowed an extra time to combine hydrogen and oxygen ions, which resulted in the evolution of H_2/O_2 gases. Such an event can cause a decrease in coulombic efficiency of the system. On the other hand, the application of fast scan rates (e.g., 100 mV/s) or higher current densities resulted in a shift in the gas evolution potential toward a higher value. As a result, we did not observe any steep increase in the current values. Due to the above explained phenomena, the assembled ASC device exhibited a relatively low coulombic efficiency (higher charging time) at low current densities.

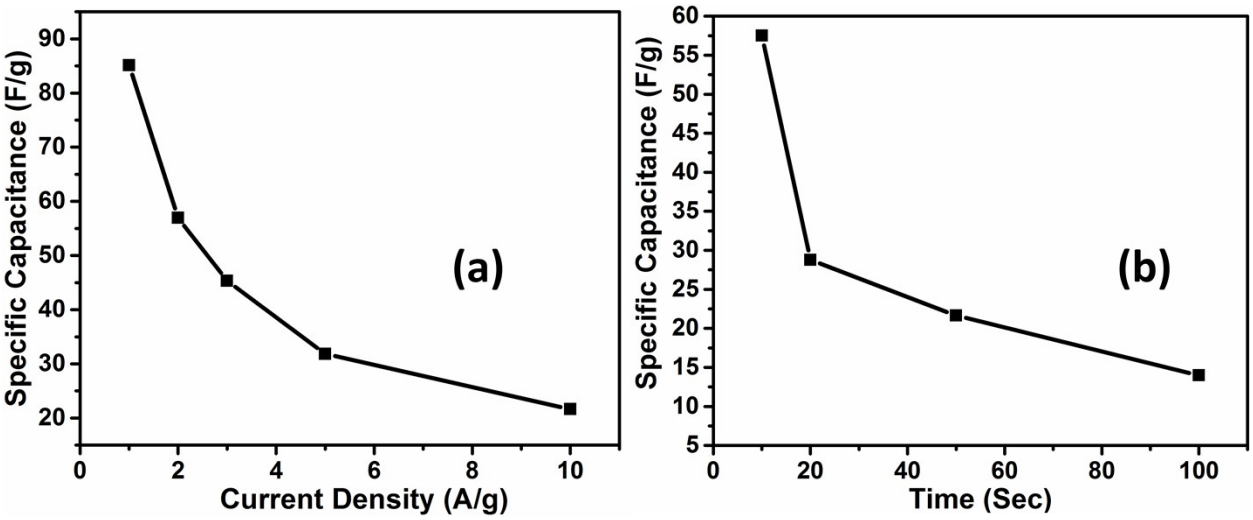

Figure S12. Variation of specific capacitance of HASD (a): As a function of current density; (b) As a function of scan rate.

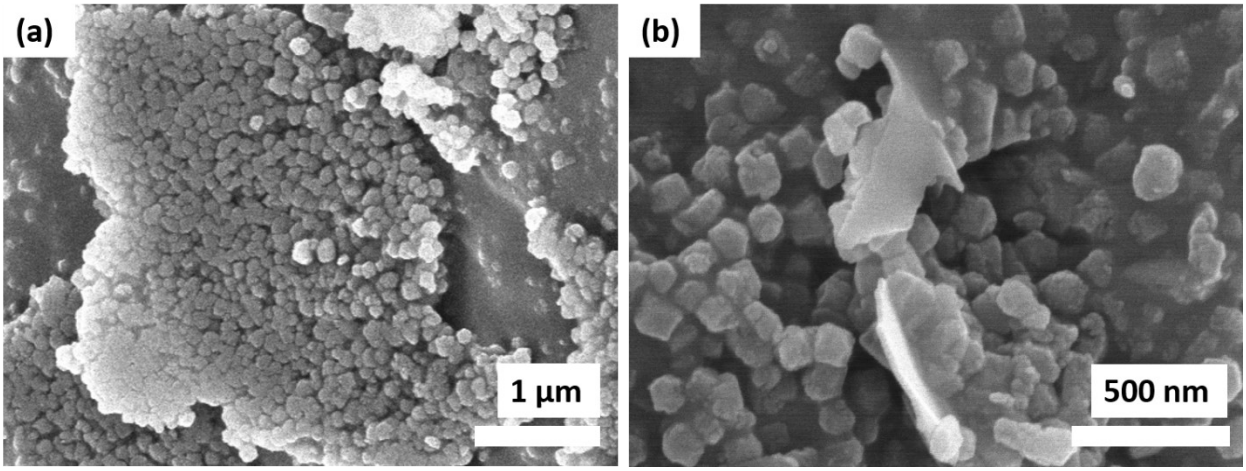

Figure S13. FESEM image of ZFC electrode (a) before charging-discharging cycling, (b) after 4000 charging-discharging cycling.

Table S2. A comparison of performance of HASD with other similar systems reported earlier

Supercapacitor Device	Electrolyte	Energy Density (Wh/kg)	Power Density (kW/kg)	Ref
MOF-derived $Co(OH)_2$//AC	6 M KOH	13.6	0.14	[7]
MIL-100 (Fe) derived Fe_3O_4/Fe/C//MIL-100 (Al) derived NPC	6 M KOH	17.49	0.388	[8]
Ni_3S_2/MWCNT-NC//AC	2 M KOH	19.8	0.798	[9]
ZIF-8/Pani	1 M H_2SO_4	21	0.1	[10]
MOF derived NiO@400//AC	3 M KOH	21.4	0.375	[11]
ZIF-8 derived AQ functionalized Carbon// NQ and TCBQ functionalized Carbon	1 M H_2SO_4	23.5	0.7	[12]
ZIF-8 derived ZnO QDs/carbon/CNTs// N-doped carbon/CNTs	1 M Na_2SO_4	26.8	0.847	[13]
Ni-Zn-BDC derived NiS_2/ZnS	3 M KOH	28	0.748	[14]
MOF-derived Co/C/$Ni(OH)_2$//AC	6 M KOH	33.6	0.516	[15]
Ni-MOF/CNT//rGO-gC_3N_4	6 M KOH	36.6	0.48	[16]
ZIF-8 derived ZLC//ZFC	**1 M Na_2SO_4**	**38.3**	**0.92**	**This work**

***AQ=** Anthraquinone**, NQ=** 1, 4-naphthoquinone**, TCBQ=** tetrachlorobenzoquinone

References

1. A. Schejn, L. Balan, V. Falk, L. Aranda, G. Medjahdi and R. Schneider, *CrystEngComm*, 2014, **16**, 4493-4500.
2. H. Kaur, G. C. Mohanta, V. Gupta, D. Kukkar and S. Tyagi, *Journal of Drug Delivery Science and Technology*, 2017, **41**, 106-112.
3. S. Sundriyal, V. Shrivastav, M. Sharma, S. Mishra and A. Deep, *Journal of Alloys and Compounds*, 2019, **790**, 377-387.
4. M. Thommes, K. Kaneko, A. V. Neimark, J. P. Olivier, F. Rodriguez-Reinoso, J. Rouquerol and K. S. Sing, *Pure and applied chemistry*, 2015, **87**, 1051-1069.
5. J. Chmiola, G. Yushin, Y. Gogotsi, C. Portet, P. Simon and P.-L. Taberna, *science*, 2006, **313**, 1760-1763.
6. A. N. Banerjee, V. Anitha and S. W. Joo, *Scientific reports*, 2017, **7**, 1-20.
7. Z. Wang, Y. Liu, C. Gao, H. Jiang and J. Zhang, *Journal of Materials Chemistry A*, 2015, **3**, 20658-20663.
8. A. Mahmood, R. Zou, Q. Wang, W. Xia, H. Tabassum, B. Qiu and R. Zhao, *ACS applied materials & interfaces*, 2016, **8**, 2148-2157.
9. C.-S. Dai, P.-Y. Chien, J.-Y. Lin, S.-W. Chou, W.-K. Wu, P.-H. Li, K.-Y. Wu and T.-W. Lin, *ACS applied materials & interfaces*, 2013, **5**, 12168-12174.
10. R. R. Salunkhe, J. Tang, N. Kobayashi, J. Kim, Y. Ide, S. Tominaka, J. H. Kim and Y. Yamauchi, *Chemical science*, 2016, **7**, 5704-5713.
11. M. K. Wu, C. Chen, J. J. Zhou, F. Y. Yi, K. Tao and L. Han, *Journal of Alloys and Compounds*, 2018, **734**, 1-8.
12. B. Guo, Y. Yang, Z. Hu, Y. An, Q. Zhang, X. Yang, X. Wang and H. Wu, *Electrochimica Acta*, 2017, **223**, 74-84.
13. Y. Zhang, B. Lin, J. Wang, J. Tian, Y. Sun, X. Zhang and H. Yang, *Journal of Materials Chemistry A*, 2016, **4**, 10282-10293.
14. G.-C. Li, M. Liu, M.-K. Wu, P.-F. Liu, Z. Zhou, S.-R. Zhu, R. Liu and L. Han, *RSC advances*, 2016, **6**, 103517-103522.
15. X. Li, Y. Qiao, C. Wang, T. Shen, X. Zhang, H. Wang, Y. Li and W. Gao, *Journal of Alloys and Compounds*, 2019, **770**, 803-812.
16. P. Wen, P. Gong, J. Sun, J. Wang and S. Yang, *Journal of Materials Chemistry A*, 2015, **3**, 13874-13883.